MALACHITE GREEN ADSORPTION FROM AQUEOUS MEDIUM BY CHITOSAN ASSISTED SILVER NANOPARTICLES (AgNPs): ISOTHERM AND THERMODYNAMICS STUDIES

Akeem Adesina Bamigbade[1*], Kayode Damilare Oduntan[1], Sulaiman Tofunmi Ruth[1], Ayeni Itunu[1], Kolawole Olubumi Akiode[2], Mohamed Hefnawy[3], Ali El Gamal[4], Talha Bin Emran[5,6], and Andrew Edwin Ofudje[7]

[1]Department of Chemistry, College of Physical Sciences, Federal University of Agriculture, Abeokuta, PMB 2240, Alabata Road, Abeokuta, Nigeria
[2]Department of Chemistry, Nigeria Army University Biu, PMB 1500, Borno State, Nigeria.
[3]Department of Pharmaceutical Chemistry, College of Pharmacy, King Saud University, Riyadh 11451, Saudi Arabia
[4]Department of Pharmacognosy, College of Pharmacy, King Saud University, Riyadh 11451, Saudi Arabia
[5]Department of Pathology and Laboratory Medicine, Warren Alpert Medical School, Brown University, Providence, RI 02912, USA
[6]Department of Pharmacy, Faculty of Health and Life Science, Daffodil International University, Dhaka 1207, Bangladesh
[7]Department of Chemical Sciences, Mountain Top University, Ogun State, Nigeria

ABSTRACT. The contamination of water by toxic, non-biodegradable dyes like malachite green (MG) presents serious environmental and health risks, demanding effective and sustainable removal strategies. This study explores the adsorption of MG from aqueous solutions using silver nanoparticles (AgNPs) as adsorbents. The synthesized AgNPs were characterized using FTIR, XRD, UV-Visible spectrophotometry, and SEM. XRD confirmed a face-centered cubic crystalline structure, while SEM images showed both spherical and irregular granular shapes. FTIR spectra displayed peaks between 1005 and 1646 cm^{-1}, indicating phosphonate bond formation between $-NH_3^+$ groups of chitosan and $-PO_3^{2-}$ moieties of sodium tripolyphosphate (NaTPP) during cross-linking. Adsorption experiments revealed that all tested factors significantly affected MG uptake by the AgNPs, demonstrating their potential for effective dye removal from aqueous environments. AgNPs effectively remove MG in acidic conditions of pH of 4.7, contact time of 80 min, and temperature of 45 °C, indicating that electrostatic interactions primarily drive. The adsorption models were best described by Tempkin isotherms. The findings suggest that AgNPs are promising adsorbents for MG removal from aqueous environments.

KEY WORDS: Malachite green (MG), Silver nanoparticles (AgNPs), Sodium tripolyphosphate, Adsorption, Cross-linking, Electrostatics attraction

INTRODUCTION

Nanoparticles are extremely small particles that measure between one and a hundred nanometers in size [1]. Although they cannot be observed with the naked eye, they possess numerous arrays of potential uses across many fields for instance materials science, electronics, optics, medicine, and catalysis, all of which could enhance human health [2, 3]. The exceptional characteristics of nanoparticles, including their great surface area to volume ratio, well-ordered size, form, and distribution, make them particularly suitable for diverse applications [3]. Among the numerous forms of nanoparticles, noble metals nanoparticles are especially valuable in the biomedical sector, finding uses in bio-imaging, sensors, diagnostics, and novel therapies [4]. Due to their

––––––––––

numerous advantages over their bulk counterparts, including distinctive optical, physical, and chemical reactivity, metal nanomaterials are increasingly being utilized as subjects of various research [5]. Applications for metal nanomaterials comprise colorimetric devices for many analytes [6, 7], antimicrobials [8], conductors [9], antibacterial agents [10], and energy conservation technology [2].

Silver nanoparticles (AgNPs) belong to the most frequently used materials. Unlike other metals, AgNPs exhibit unique characteristics in terms of size, shape, and exceptional thermal conductivity [11]. Additionally, AgNPs are more cost-effective than many other metals and possess significant physical properties, favorable chemical reactivity, and relatively high availability [12]. Consequently, they are employed in a broad range of applications. With a low menace of toxicity to beings, AgNPs, have recently been incorporated as antimicrobial mediators in countless products, including water purification systems [13], wound dressings [14], animal feed [15], cosmetics [16], and catheters coating [17], all with minimal risk of human toxicity. Numerous procedures have been developed for the production of AgNPs including chemical reduction [18] and the utilization of Ketapang leaves [19], the use of *Syzygium polyanthum* extract [20], and the use of Neem bark extract [21]. Sodium borohydride can serve as a reducing agent when creating AgNPs through chemical reduction [22].

The AgNPs, alternatively, are not highly stable and readily aggregate to create larger flocks. To stop the aggregation of AgNPs between their surfaces, additional materials are required as a capping agent [23]. AgNPs stability, electro-optical characteristics, and biological uses can all be enhanced by stabilizing them with a polymer. Polymers can attach to metal nanoparticle surfaces by a variety of interactions, including hydrophobic, electrostatic, and chemical adsorption [24]. Poly-(vinylpyrrolidone) (PVP) [25], and hyperbranched polyethyleneimine (PEI) [3] are polymers that can be utilized as stabilizers for AgNPs. In this study, chitosan was employed as a silver nanoparticle capping agent. N-acetylglucosamine and D-glucosamine make up the linear polymer called chitosan. The $-NH_2$ group in chitosan can interact with the silver nanoparticle surface.

An organic compound referred to as malachite green (MG) finds applications extensively across various industries, particularly for dyeing paper, leather, silk, and plastics. However, its presence in the environment (especially, wastewater) poses significant health risks, including respiratory toxicity, reduced fertility in humans, and harmful effects on both humans and animals upon ingestion or inhalation. Additionally, MG can cause skin irritation, is classified as carcinogenic, and is highly toxic to mammalian cells [20, 25]. Therefore, it is imperative to remove MG from wastewater to safeguard the environment [26]. Despite its extraordinary resistance to light and reduction, traditional techniques for instance chemical precipitation and biological treatment have proven ineffective in eliminating this compound [27]. The resistance of these dyes to microbial degradation renders conventional biological treatment methods inadequate for wastewater treatment. Moreover, as the concentration of effluent increases, the effectiveness of physic-chemical treatment methods diminishes. The solidity of its chemical structure, along with the bio-compatibility, robust oxidizing properties, non-poisonous, and cost-effectiveness of metal precursors, has positioned silver as a promising semiconductor for the elimination of various toxic organic contaminants via adsorption and photo-catalytic processes [5, 6, 8, 18]. Recently, improvements in nanotechnology have been leveraged for wastewater remediation [9, 15, 17].

The AgNPs exhibit enhanced reactivity due to their extensive surface area [1, 4], and enhanced reactivity due to their extensive surface area [1-3]. The selection of this study was primarily driven by growing environmental concerns regarding the contamination of water bodies by toxic dyes like MG. MG is a widely used synthetic dye in the textile, paper, and aquaculture industries, but its persistence in water sources poses serious ecological and health risks due to its toxicity and carcinogenic nature [18]. Addressing this issue necessitates the development of efficient and sustainable removal techniques. Traditional water treatment methods, often have limitations in

terms of cost, efficiency, and environmental impact [11, 18].

Nanotechnology presents an innovative solution to this problem, with AgNPs emerging as promising candidates for pollutant removal due to their high surface area, tunable physicochemical properties, and strong adsorption capabilities [4, 8, 11, 12]. Their unique properties make them effective in interacting with dye molecules, facilitating enhanced adsorption and removal from aqueous solutions. Similarly, the study was informed by the increasing demand for sustainable and eco-friendly water treatment solutions and the use of bio-facilitated synthesis methods for AgNPs aligns with global efforts to develop green technologies that minimize environmental harm while ensuring cost-effectiveness. The primary objective of this research is to synthesize and characterize chitosan-assisted AgNPs (Ch-AgNPs) using various analytical techniques such as Fourier Transform Infrared Spectroscopy (FTIR), X-ray diffractometry (XRD), UV-Visible spectrophotometry, and scanning electron microscopy (SEM). The efficiency of Ch-AgNPs in removing MG from aqueous solutions under different conditions was determined. Furthermore, the research seeks to analyze the adsorption behavior using established isotherm models, including Langmuir, Freundlich, and Tempkin, to understand the nature of MG adsorption onto Ch-AgNPs.

EXPERIMENTAL

Chemicals and reagents

Chitosan derived from lobster shell waste, exhibiting a degree of deacetylation of 85%, was sourced from Sigma Aldrich, India, along with HCl, glacial acetic acid, and NaOH. Sodium tripolyphosphate (NaTTP), sodium borohydride, acetone, ethanol, and silver nitrate were procured from Sigma Aldrich, India, and utilized as supplied. MG was supplied by Bektoh Germany and was employed as received. Its visible spectrum indicated a molar extinction coefficient of 619 nm. All chemicals were utilized without additional decontamination, and all solutions were made using distilled water. Characterization of AgNPs was conducted using various atomic and scanning techniques, comprising X-ray diffractometry (XRD) (Philips PAN analytical model, Netherlands), Fourier transform infrared spectroscopy (FTIR) (ABBBOMEM MB 3000 instrument, Canada), scanning electron microscopy (SEM) (NOVA Nano JSM-6480 LV model, Japan), and UV-Visible Spectrophotometry (Shimadzu UV-spectrophotometer (UV-1800, Japan).

Synthesis of AgNPs and AgNO₃/chitosan-NaTPP

The AgNP was synthesized following modified procedures from the literature [28, 29]. Initially, 60 mg of chitosan was added to 20 mL of 2% acetic acid to create a chitosan solution. Subsequently, a 0.25% NaTPP solution was incorporated into the chitosan solution in a 1:3 ratio, with gentle stirring until an opalescent suspension was formed. Following this, 10 mL of 0.3% $AgNO_3$ was added to the chitosan-NaTPP hydrogel (serving as a capping agent), and the mixture was stirred continuously for 30 min to achieve a homogeneous solution. Finally, 10 mL of 0.01 M $NaBH_4$ was added to the mixture. The synthesis was carried out at room temperature of 25 °C and in a slightly acidic medium (pH of 6.0). The AgNPs were then separated from the liquid through centrifugation at 10,000 g for 1 h. The supernatant was removed, and the AgNPs formed were carefully washed with acetone, ethanol, and distilled water before being vacuum-filtered. The resulting AgNPs were dried in an oven at 115 °C. The proposed mechanism for the synthesis of AgNPs in Figure 1 was adopted from the reported work of Leonida *et al*. [28] with minor modifications.

Figure 1. Reaction mechanism for chitosan-AgNPs synthesis at 25 °C and slightly acidic medium (pH of 6.0).

Adsorption studies

A stock solution of MG dye was made by adding 0.1 g of MG in 100 mL of water, giving rise to 100 mg/L concentration. A working solution of 50 mg/L MG was formed from this stock solution. Subsequently, 0.02 g of AgNPs was introduced as adsorbent to each of the prepared solutions and then the mixtures were stirred for 2 h. The absorbance of the prepared dye solution was determined at 420 nm, the maximum wavelength (λ_{max}), using Shimadzu UV-spectrophotometer (UV-1800, Germany). The equilibrium quantity of MG adsorbed (q_e) in mg/g was evaluated by applying equation (1) below, based on absorbance measurements taken before and after the adsorption process, as well as considering the influence of concentration, temperature, time, pH, and adsorbent dosage.

$$q_e = \left(\frac{C_o - C_e}{m} \right) \times v \tag{1}$$

In this context, v denotes the volume of the solution utilized (mL), m signifies the weight of the adsorbents (g), and C_o and C_e represent the initial and final concentration of the adsorbates (mg/L), respectively. The impact of temperature was assessed within a range of 10 °C to 40 °C, while the influence of time was evaluated at 10 min intervals spanning from 10 to 90 min. To explore the effect of concentration, adsorbate levels ranging from 20 to 250 mg/L were employed, and pH was adjusted between 2 and 13 using either 0.1 M HCl or 0.1 M NaOH.

Desorption experiment

Following the adsorption of MG onto AgNP, the AgNP adsorbent was separated from the MG solution by dipping the used adsorbent in 0.1 M HCl as a desorbing agent. Afterward, the adsorption cycle was carried out after a pre-determined time, the solution mixture was filtered and the solution was analyzed for MG concentration by measuring the absorbance of the filtrate using a UV-Visible spectrophotometer to determine adsorption-desorption efficiency. The AgNPs adsorbent was regenerated by washing with 0.1 M HCl and water which was subsequently applied in adsorption cycles to evaluate its reusability. The efficiency of desorption was determined using Equation 2:

$$\text{Desorption Efficiency} = \frac{\text{Amount of MG Desorbed}}{\text{Amount of MG Adsorbed}} \times 100 \tag{2}$$

The experiment was conducted in triplicate and the average value was reported.

Characterizations of the adsorbent

The UV-Visible spectrum of the brown solution of AgNPs that results from the excited particles' surface plasmon vibrations was recorded on a Shimadzu UV-160 double-beam spectrophotometer. The FTIR spectrum was documented in KBr pellets for AgNPs at 25 °C using an ABBBOMEM MB 3000 instrument. The SEM images of the chitosan-stabilized AgNP were observed with the Hitachi SU 6600 instrument. To evaluate the phase variation and particle size of the produced AgNPs X-ray diffraction spectrophotometry (Philips PAN analytical) was engaged. The produced nanoparticle was investigated using Cu-Kα radiation at a voltage of 35.0 kV and a current of 25.0 mA with a scan rate of 0.05 °/s and λ = 1.55 Å. To investigate the morphological characteristics of AgNPs produced NOVA Nano Scanning Electron Microscope (JSM-6480 LV) was employed. The solutions were smeared across slides to create the SEM slides. To make the samples conductive, a tiny layer of platinum was applied. The samples were then analyzed with SEM at a high-speed voltage of 6.0 KV, emission current of 78 – 82 A, and a short distance of 8 – 15 nm.

RESULTS AND DISCUSSION

X-ray diffraction spectrum of AgNPs analysis

The phase configuration and particle unit of the produced AgNPs were analyzed using XRD. Figure 2 illustrates the XRD spectrum of the hybrid derivative from AgNPs. The synthesized AgNPs exhibit a cubic face-centered structure, as evidenced by the presence of four distinct diffraction peaks at 2θ values of 39.09°, 45.15°, 65.67°, and 78.54°, corresponding to the Bragg reflections indexed as 111, 200, 220, and 311, respectively [30] confirming the crystalline nature of the AgNPs. These data align with JCPDS card no. (65-2871), and the pronounced sharpness of the peaks further substantiates the crystalline characteristics of the particles [31]. The crystallite size of the synthesized AgNPs was evaluated with a value of 15 nm employing Debye-Scherrer expression ($D = k\lambda/\beta\cos\theta$), with a relative deviation of 4.55%. In this equation, D represents the average crystallite size, k is the Scherrer-Scherer constant valued at 0.85, λ represents the wavelength of the X-ray sources (0.16402 nm), θ is the Bragg angle, and β is the angular full-width at half maximum (FWHM = 0.005) of the XRD peak at the specified diffraction angle [32]. The XRD pattern (JCPDS, File No- 04-0783) confirms that the synthesized AgNPs configuration is a face-centered cubic (FCC).
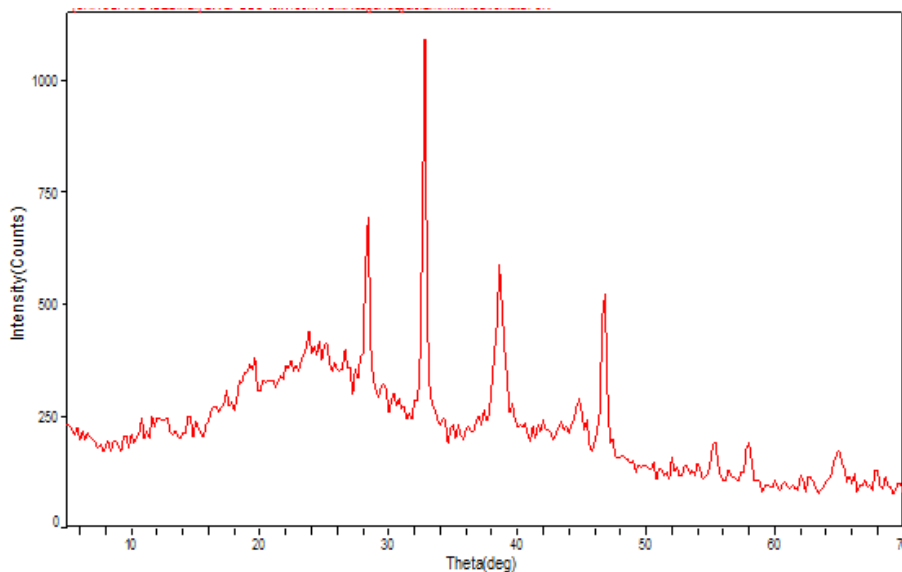
Figure 2. XRD spectrum of silver nanoparticle (AgNPs).

SEM analysis of AgNPs

The AgNP's morphological arrangement was examined using scanning electron microscopy (SEM). The image magnification results of AgNPs at an 80 nm scale with a high voltage of 5.0 kV are presented in Figure 3a. Due to the bio-mediated ionic gelation process, the AgNPs exhibit a relatively smooth, spherical structure characterized by high density and an asymmetrical granular form. This outcome agreed with the verdicts of Abdulwahid *et al.* [33], which noted that the synthesized AgNPs possess a globular shape, are slightly elongated, and demonstrate a strong tendency to aggregate, forming larger particle clusters. Figure 3b displays the AgNP's UV-visible spectrum. The AgNP's Surface Plasmon Resonance (SPR) peak, which corresponds to the greatest absorbance peak, is detected at 420 nm. Generally, it appears that the Ag^+ bio-reduction to Ag^0 was verified by the UV-visible spectrum.

UV-Visible result of AgNPs

The solution of AgNPs, characterized by its brown color, was generated through the excitation of surface Plasmon vibration. This solution underwent UV-visible spectral analysis and the UV-Visible spectra of the AgNPs is illustrated in Figure 3b. The peak corresponding to the surface plasmon resonance (SPR) of the AgNPs, indicates the maximum absorbance, which was observed at approximately 420 nm. The absorbance and the broadening of the peak near 420 nm suggest that the nanoparticles are mono-dispersed, reflecting the SPR absorption band resulting from the collective vibration of electrons in resonance with UV-visible light [34] indicating that Ag^+ bio-reduction to metallic silver.
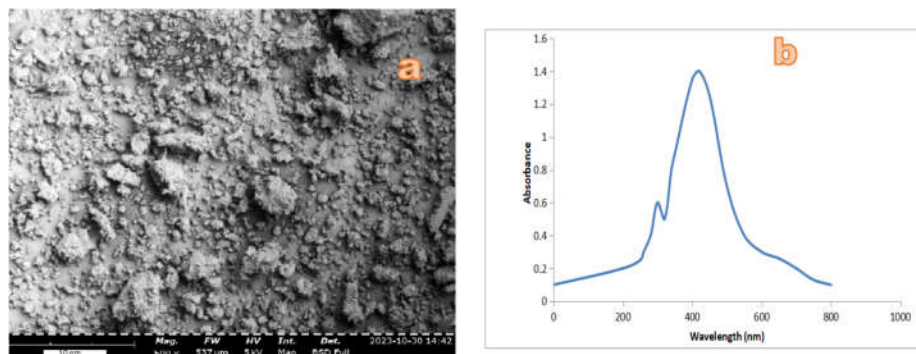
Figure 3. (a) Scanning electron micrograph (SEM) of AgNPs, and (b) UV-Visible spectrum of AgNPs.

FT-IR result of AgNPs

The FT-IR spectrum of the AgNP derivative is presented in Figure 4. The spectrum of the AgNPs gave peaks within the range of 1055-1645 cm^{-1}, which indicates the existence of phosphonate bonds formed between the $-NH_3^+$ groups of chitosan and the $-PO_3^{2-}$ groups of NaTPP in the course of the cross-linking procedure. Notably, two peaks are observed at 1141 cm^{-1} and 1279 cm^{-1}, corresponding to the symmetric and asymmetric stretching of the phosphonate link, separately. Additionally, the asymmetric peak is attributed to limited rotation [35]. The two terminal $-PO_3^{2-}$ groups of the NaTPP molecules appear to be linked to two $-NH_3^+$ (CH_3COO^-) groups from two chitosan monomers. The broadening, along with the loss of minor features in the band, suggests an increase in intermolecular hydrogen bonding between NH and OH groups. The maximum peak is observed at nearly 3880 cm^{-1} for the AgNPs. This band broadening aligns with the past literature findings regarding chitosan-NaTPP nanoparticles and chitosan succinylated nanoparticles [36]. This is ascribed to the creation of hydrogen-linked networks. AgNPs display a low-intensity yet wide band centered near 3265 cm^{-1}, indicating that the Ag-chitosan complexes primarily consist of nanoparticles.

Adsorption results

Contact time effect

To evaluate the equilibrium time for the adsorption processes, the effect of contact time on the adsorption of MG onto AgNPs was examined at a pH of 8.0 utilizing an MG concentration of 50 mg/L and AgNPs dose of 0.02 g over a period ranging from 10 to 90 min. The adsorption effectiveness of AgNPs improved progressively with longer contact times, attaining a maximum after 60 min (Figure 5a). Subsequently, the adsorption of the MG onto the AgNPs remained stable. This initial increase in adsorption can be primarily attributed to the accessibility of adsorption spots, which becomes unavailable over time in the course of the adsorption, leading to a negligible increase in further adsorption onto the adsorbents [37].

Effect of pH

Figure 5b demonstrates the effect of pH on the adsorption capacity of MG onto AgNPs. pH was varied from 2 to 13 applying 0.1 M HCl or 0.1 M NaOH to adjust the pH during the experimental

procedure, and the effects were assessed by measuring the equilibrium concentrations of the AgNPs (*i.e.*, 25 mg/L) for 80 min. The adsorption of MG onto AgNPs increased with rising pH levels, achieving optimal sorption at approximately pH 4.7, a trend that can be attributed to the enhanced degradation of the MG dye. There was a complete acid-base neutralization reaction that led to the negative charges on the surface of the silver nanoparticle being neutralized by MG, which facilitated diffusion phenomena and created additional active sites for adsorption. Consequently, the adsorption mechanism is primarily governed by the electrostatics interactions [37]. However, at a pH level below 4, there was a notable reduction in the quantity of negatively charged spots on the AgNPs, leading to a substantial decline in the degree of dye degradation. The increase in positively charged active sites on the surface resulted in greater repulsion between the dye and the AgNPs, thereby diminishing the efficiency of the adsorption phenomenon.
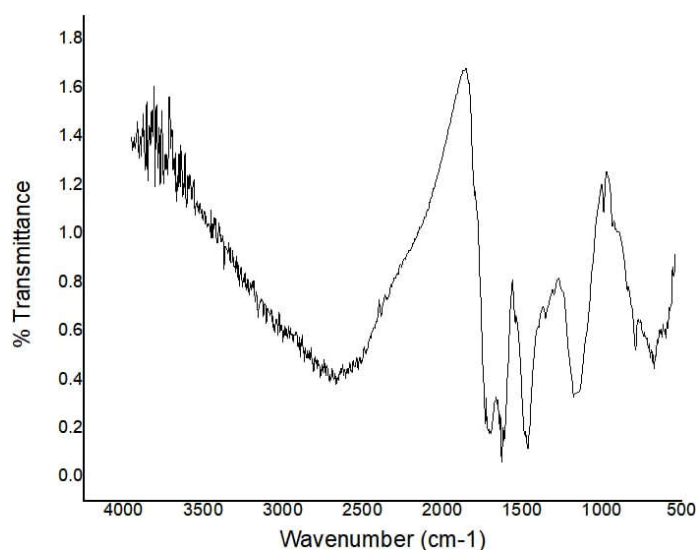

Figure 4. The FTIR spectrum of AgNPs.

In acidic conditions, MG adsorption was enhanced, but as pH increased, the adsorbent surface became more negatively charged, which contributed to an increase in adsorption capacity due to electrostatic interactions. Conversely, at elevated pH levels, a decrease in MG adsorption was observed. Notably, at pH 7, an increase in pH correlated with a reduction in the sorption process. This diminished adsorption may be attributed to the interactions between the AgNPs and MG being overshadowed by the bonding between the -COOH moieties of chitosan in the capped nanoparticles and water [38]. The cumulative effects of these factors strongly indicate that the pH of the solution represents an essential element in the adsorption of MG [39].

Temperature effect and thermodynamic study

The temperature influence on the adsorption of MG dye onto AgNPs was examined by utilizing the equilibrium solution concentration for each adsorbent. Adjusting the temperature from 10 to 40 °C, for 80 min for each experimental trial, the results of exercise, illustrated in Fig. 6a, showed that temperature increases had a positive influence on the adsorption procedure as more MG were adsorbed at higher temperatures [40, 41].
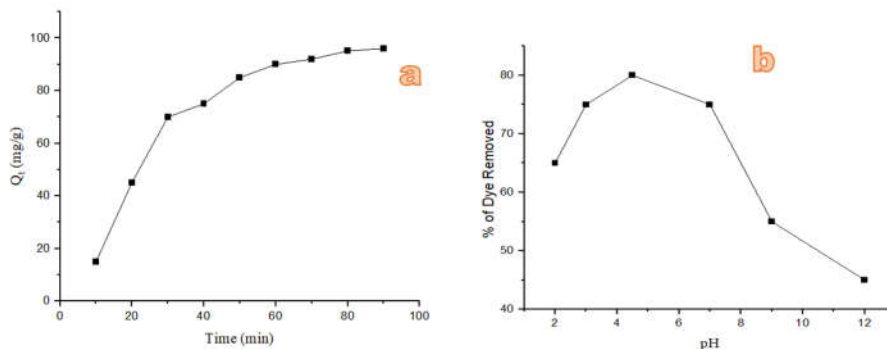
Figure 5. Plots of the (a) amount of dye removed against time, and (b) the percentage of dye removed with pH at the temperature of 45 °C, MG concentration of 50 mg/L, and AgNPs dose of 0.02 g.
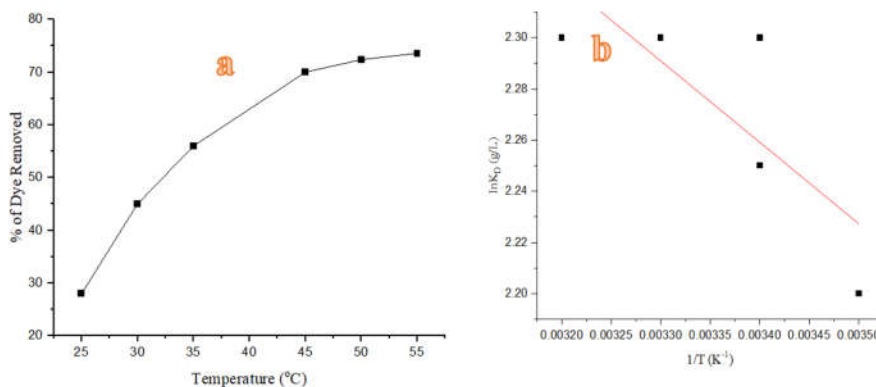

Figure 6. Plots of (a) percentage dye removed with temperature, and (b) thermodynamics at the temperature of 25 to 45 °C, MG concentration of 50 mg/L and AgNPs dose of 0.02 g, pH of 4.7, and contact time of 80 min.

Thermodynamic quantities comprising free energy change (ΔG°) (kJ/mol), enthalpy change (ΔH°) (kJ/mol), and entropy change (ΔS°) (J/K/mol) for the adsorption processes were appraised by applying the Van't Hoff equation and shown in Figure 7b [40, 41]:

$$\log K_o = \frac{\Delta S^\circ}{2.303R} - \frac{\Delta H^\circ}{2.303RT} \tag{3}$$

$$\Delta G^\circ = \Delta H^\circ - T\Delta S^\circ \tag{4}$$

$$K_o = \frac{C_{Solid}}{C_{liquid}} \tag{5}$$

The values of ΔH° (kJ/mol) and ΔS° ((J/K/mol) were obtained from the slope and intercept of the plot of $\log K_o$ against (1/T) (Figure 6b). The derived outcomes are 6.1041 kJ/mol and 27.84 (J/K/mol), respectively. Positive ΔH° value specifies that the adsorption process is endothermic,

suggesting a physiosorption mechanism. Furthermore, the positive $\Delta S°$ value implies that the adsorption process is driven by entropy, reflecting an upsurge in disorder and randomness at the interface between the solid and solution phases of the adsorbents. Water molecules that are expatriated by MG acquire additional translational entropy, which exceeds the entropy lost by dye molecules, thereby enhancing the overall randomness within the system [42]. The calculated $\Delta G°$ (kJ/mol) at room temperature is -2.192 kJ/mol. The negative $\Delta G°$ value signifies that the adsorption process is highly feasible and spontaneous. Consequently, it can be concluded that physisorption is the more effective mechanism.

Equilibrium adsorption isotherm studies

Various isotherm models, such as Langmuir, Freundlich, Tempkin, and Dubinin-Radushkevich (D-R) models, were utilized to investigate the equilibrium properties of the adsorption phenomenon. The graphs representing the isotherms are presented in Figures 7a-d, while Table 1 summarizes the constant factors associated with the isotherm equations relevant to the adsorption process. From the Langmuir isotherm (Figure 7a), the slope and intercept derived from the graph of C_e/q_e versus C_e were utilized to calculate the Langmuir adsorption constant (K_a) value (L/mg) and the hypothetical maximum adsorption ability Q_m (mg/g), which are gotten from the linear representation of the Langmuir adsorption isotherm isotherm. According to the Langmuir model, it is clear that no interaction between the adsorbate molecules occurred, and the adsorption occurs as a monolayer on a solid surface with a defined amount of equivalent spots [37, 43].

For 0.02 g of each adsorbent, the fit of the experimental data was evaluated. The AgNPs have a strong correlation coefficient of 0.9845 at the optimal concentration providing substantial evidence that the adsorption results align with the Langmuir isotherm. The Langmuir monolayer capacity indicates maximum significant adsorption of 58.45 mg of MG per gram of AgNP adsorbents. To further validate this finding, the separation factor (R_L) was evaluated to determine whether the adsorption of MG as described by the Langmuir model was favorable or unfavorable. An R_L value ranging from 0 to 1 signifies a favorable adsorption process [43]. The R_L values for the AgNPs adsorbents were found to be below 1, suggesting effective adsorption and confirming the suitability of the Langmuir isotherm to the experimental facts.

In the case of the Freundlich isotherm, the plot of lnq_e against lnC_e provided the slope and intercept necessary to ascertain the parameters of the Freundelich isotherm, expressed as K_f (mg/g)/(mg/L) and 1/n (Figure 7b). Freundlich constant shows the degree of adsorption, while the heterogeneity factors (1/n) reflect the efficiency of adsorption. The 1/n values of this factor range from 0 to 1. A 1/n value of one denotes a linear adsorption process, whereas a 1/n value below one suggests that the adsorption is chemically driven. Conversely, a 1/n value exceeding one indicates a physically driven adsorption process [37, 41, 43]. The observed Freundlich constant obtained is 0.9756 for the entire adsorbent doses confirming that the Freundlich isotherm aligns well with the experimental facts. Additionally, the value of 0.49 signifies a favorable adsorption process, highlighting the robust attraction of MG for adsorption onto AgNPs. The heat of adsorption and the interface between AgNPs and MG were assessed using the Tempkin isotherm (Figure 7c). In this context, the Tempkin constant is associated with the heat of adsorption (J/mol), T represents the absolute temperature (K), R is the gas constant (8.314 J/K/mol), and the equilibrium binding constant (K_T) is expressed in L/mg. Tempkin constant yielded a value of 8.02, with a correlation coefficient of 0.9889, which is higher than those values obtained from the Freundlich and Langmuir models. Consequently, the Tempkin model best described the experimental results, compared to both the Langmuir and Freundlich isotherms.
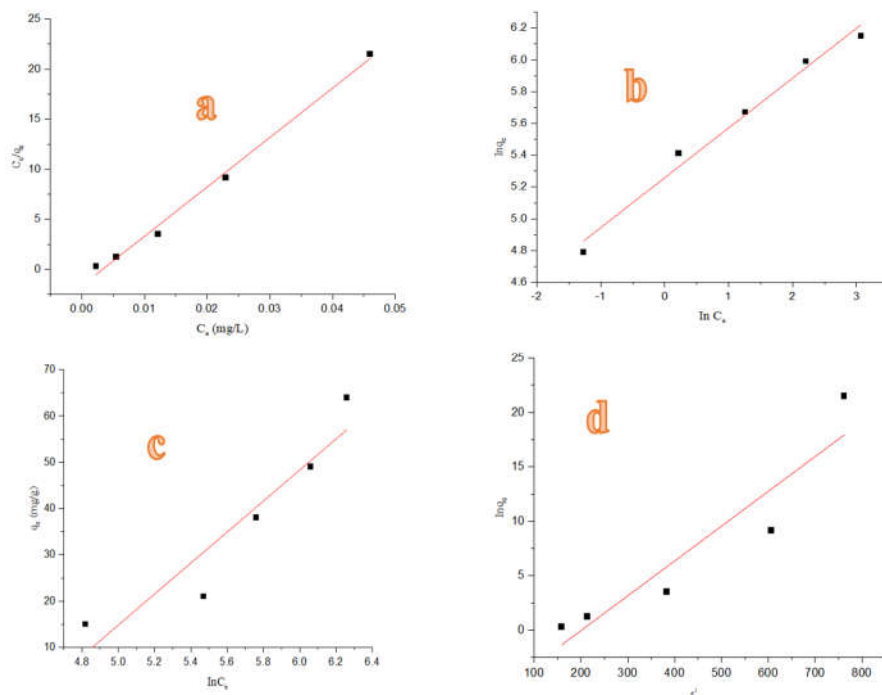
Figure 7. Plots of (a) Langmuir, (b) Freundlich, (c), Tempkin, and (d) D-R isotherms at the temperature of 45 °C, MG concentration of 29 25 mg/L and AgNPs dose of 0.02 g, pH of 4.7 and contact time of 80 min.

Table 1. The constants isotherm factors for MG adsorption onto AgNPs.

Isotherms	Equations	Constants	Adsorbents AgNPs
Langmuir	$$\frac{C_e}{q_e} = \frac{1}{K_a Q_e} + \frac{C_e}{Q_e}$$	Q_e(mg/g) K_a(L mg^{-1}) R_L R^2	58.80 0.54 0.07 0.9834
Freundlich	$$\ln q_e = \ln K_f + \left(\frac{1}{n}\right)\ln C_e$$	K_f n 1/n R^2	6.38 2.02 0.49 0.9746
Tempkin	$$q_e = B_1 \ln K_T + B_1 \ln C_e$$	B_1 (mg/g) K_T R^2	12.65 8.01 0.9889
Dubinin-Radushkevic	$$\ln q_e = \ln Q_s - B\varepsilon^2$$	Q_s E (kJ/mol) B R^2	212.14 814.25 -223.28 0.3817

The D-R isotherm was utilized to assess the permeability, actual free energy, and adsorption characteristics. The term K (mol^2/(kJ^2)) denotes a constant linked to the adsorption energy, while Q_s (mg/g) signifies the hypothetical saturation capacity, and the Polanyi potential (*e*) is also

included. The slope of the plot of the Polanyi potential against the corresponding variable, i.e. $\ln q_e$ versus ε^2 in Figure 7d yields the B value, whereas the intercept gives the Q_s value. In this case, the D-R model demonstrates a suboptimal fit to the experimental results concerning AgNPs. The fitting data indicates that the correlation coefficient for the Langmuir isotherm surpasses those of the other isotherms, implying that the Langmuir, Freundlich, and Tempkin models more accurately characterized the adsorption of MG onto the AgNPs. This suggests that the adsorption occurs as a monolayer process, whereas the Dubinin-Radushkevich isotherm is deemed unstable for this adsorption process [44]. The AgNPs have been compared with other adsorbents [45-48] on the degradation of MG from aqueous solution. Figure 8 depicts the schematic diagram illustrating the adsorption mechanism.

Table 2. Comparison of AgNPs with other adsorbents on the degradation of MG from aqueous solution.

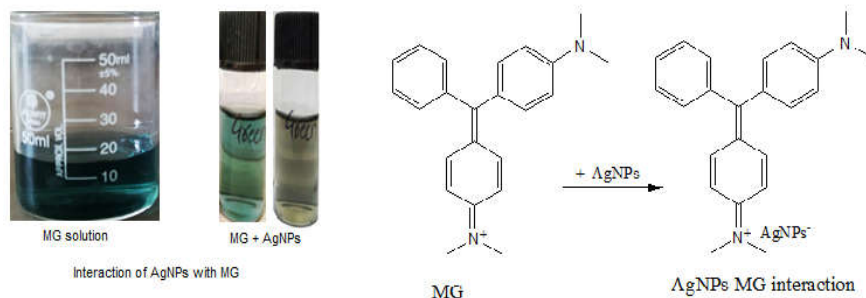| Various adsorbents	Dyes	Optimum pH	Adsorption capacity (mgg^{-1})	References
Carboxylate group functionalized multi-walled carbon nanotubes	MG	9	11.8	[45]
ZnO nanorod-loaded activated carbon	MG	6	20	[46]
Nickel hydroxide nanoplate-modified activated carbon	MG	6.5	56.9	[47]
Lignin sulphonate-based mesoporous material	MG	7	121	[48]
AgNPs (AgNPs)	MG	4.7	58.8	This work

Figure 8. Schematic diagram illustrating the adsorption mechanism.

Desorption study

The outcome of desorption of MG from AgNPs established the reusability of the AgNPs as adsorbent. The capacity of AgNPs to be reused declines over a series of cycles of use as displayed in Figure 9. These discoveries offer valuable statistics about the resilience and enduring efficiency of AgNPs as adsorbents for MG. The percentage adsorption dropped from 68.52% in the first cycle to 45.53% by the fifth cycle. Although the reduction was minimal within the first three cycles of the processes demonstrating that AgNPs can be subject to reusability after each adsorption experiment. These findings align with previous research. Yunusa and Ibrahim [49] investigated the desorption and reusability of activated carbon derived from desert date seed shells for the removal of MG (MG). Their study revealed that after five adsorption-desorption cycles,

the removal efficiency decreased from 96.5% to 70.5%. In a separate study by Pandian *et al.* [50], AgNPs (AgNPs) were employed for the removal of MG from aqueous solutions and the results from their reusability tests demonstrated a similar trend, with adsorption efficiency decreasing from 68.52% to 45.53% by the fifth cycle. Azaman *et al.* [51] observed that the desorption efficiency of MG (MG) by desert date seed shell improved as ethanol concentration increased, rising from 50% to 80%. However, a slight decline was noted when the ethanol concentration reached 90%. The highest desorption efficiency was recorded at an ethanol-to-water ratio of 80:20 (v/v).
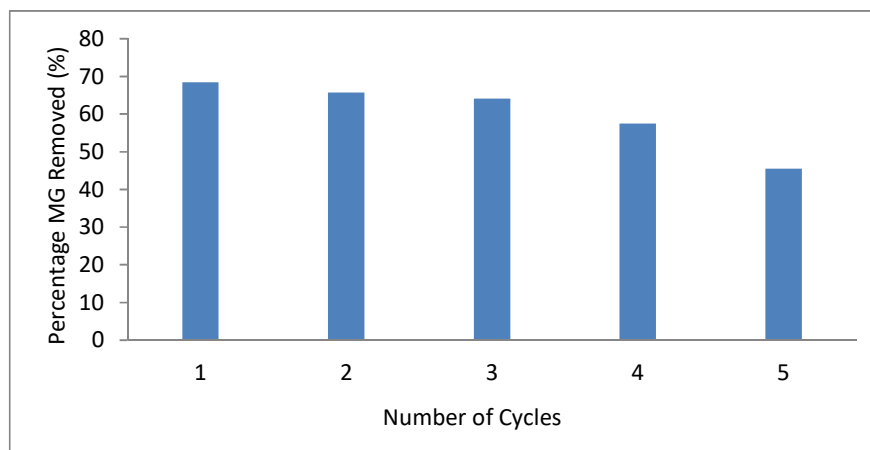

Figure 9. Chart of percentage MG removal versus number of cycles.

CONCLUSION

The AgNPs were synthesized via an ionic gelation method and characterized using SEM, XRD, UV-Vis, and FTIR. XRD analysis confirmed a face-centered cubic structure with diffraction peaks at 2θ values of 38.09°, 44.15°, 64.67°, and 77.54°. The SEM imaging revealed smooth, globular AgNPs with a tendency to form aggregated clusters due to the bio-assisted ionic gelation process. FTIR spectra showed peaks at 1055–1309 cm^{-1}, indicating phosphonate bond formation between chitosan and sodium tripolyphosphate during cross-linking. The synthesized AgNPs were used as adsorbents for MG removal from aqueous solutions, reaching equilibrium within 80 min. Optimal adsorption occurred in acidic conditions (pH of 4.7) due to acid-base interactions, with an ideal adsorbent dosage of 0.02 g. Adsorption isotherms were best described by the Tempkin models, while the Dubinin-Radushkevich model was unsuitable. These findings highlight the potential of AgNPs for effective MG adsorption, demonstrating their efficiency in water treatment applications.

Author contributions

All authors have equal contributions.

Data availability statement

All data are available in this manuscript.

REFERENCES

1. Mohammed, A.D.; Azlan, A.A.; Shaymaa, H.N.; Farhank, S.B.; Wesam, A.; Wasan, H.K.; Mahmood, S.J.; Saleh, T.A.; Mohammad, A.; Nazila, O. Sustainable green synthesis of silver nanoparticles for safer biomedical application. *J. Environm. Chem. Eng.* **2025**, 13, 115998.
2. Aboelfetoh, E.F.; Gemeay, A.H.; El-Sharkawy, R.G. Effective disposal of methylene blue using green immobilized silver nanoparticles on graphene oxide and reduced graphene oxide sheets through one-pot synthesis. *Environ. Monit. Assess*. **2020,** 192, 1-20.
3. Yang, Z.; Zhang, T.; Ren, J.; Li, J.; Ge, J.; Shan, H.; Ji, T.; Xu M.; Liu, Q. Nano-silver functionalized spherical activated carbon with enhanced dipropyl sulfide adsorption capacity and antibacterial properties. *RSC Adv.* **2022**, 12, 9933-9943.
4. Mohd, F.A.I.; Adnan, S.; Nahid, N.; Afroz, J.; Tahir, A.B.; Afreen, I. Green synthesis of silver nanoparticles: A comprehensive review of methods, influencing factors, and applications. *JCIS Open* **2024**, 16, 100125.
5. Rajamani, R.K.; Kuppusamy, S.; Bellan, C. Biosynthesis, characterization and medical aspect of silver nanoparticles against pathogenic bacteria. *MOJ Toxicol*. **2018**, 4, 103-109.
6. Mst. Sanjida, A.; Mahfuza, M.; Md. Ataur, R.; Mahmuda, A.; Rezaul, K.R.; Shamim, M.; Al Mamun, F.; Md. Tajuddin, S. A systematic review on green synthesis of silver nanoparticles using plants extract and their bio-medical applications. *Heliyon* **2024**, 10, e29766.
7. Shrivastava, V.; Ali, I.; Marjub, M.M.; Rene, E.R.; Soto, A.M.F. Nanocomposites via in-situ co-reduction of the oxides. *Powder Technol*. **2022**, 233, 208-214.
8. Khalid, N.R.; Hammad, A.; Tahir, M.B.; Rafique, M.; Iqbal, T.; Nabi G.; Hussain, M.K. Enhanced photocatalytic activity of Al and Fe co-doped ZnO nanorods for methylene blue degradation. *Ceram. Int*. **2019**, 45, 21430-21435.
9. Ahmed, T.; Noman, M.; Shahid, M.; Niazi, M.B.K.; Hussain S.; Manzoor N. Green synthesis of silver nanoparticles transformed synthetic textile dye into less toxic intermediate molecules through LC-MS analysis and treated the actual wastewater. *Environ Res.* **2020**, 191, 110-142.
10. Li, Y.; Sun, S.; Gao, P.; Zhang, M.; Fan, C.; Lu, Q.; Li, C.; Chen, C.; Lin B.; Jiang, Y. A tough chitosan-alginate porous hydrogel prepared by simple foaming method. *J. Solid State Chem.* **2021**, 294, 121-197.
11. Hussain, M.K.; Khalid, N.R.; Tanveer, M.; Kebaili, I.; Alrobei, H. Fabrication of CuO/MoO$_3$ pn heterojunction for enhanced dyes degradation and hydrogen production from water splitting. *Int. J. Hydrogen Energy* **2022**, 47, 15491-15504.
12. Nagar, N.; Devra, V. Oxidative degradation of Orange G by peroxomonosulfate in presence of biosynthesized copper nanoparticles - a kinetic study. *Environ. Technol. Innov*. **2018**, 10, 281-289.

13. Khodadadi, B.; Bordbar, M.; Yeganeh-Faal, A. Green synthesis of Ag nanoparticles /clinoptilolite using *Vaccinium macrocarpon* fruit extract and its excellent catalytic activity for reduction of organic dyes. *J. Alloys Compd.* **2017**, 719, 82-98.
14. Pandey, S.; Do, J.Y.; Kim J.; Kang, M. Fast and highly efficient catalytic degradation of dyes using κ-carrageenan stabilized silver nanoparticles nanocatalyst. *Carbohydr. Polym.* **2020**, 230, 115-127.
15. Jain, A.; Ahmad, F.; Gola, D.; Malik, A.; Chauhan N.; Dey, P. Multi dye degradation and antibacterial potential of Papaya leaf derived silver nanoparticles. *Environ. Nanotechnol. Monit. Manag.* **2020**, 14, 100337.
16. Sehar, S.; Sehrish, F.; Qurat, U.; Zunaira, S.; Muhammad, R.S. A.J. A review on green synthesis of silver nanoparticles (SNPs) using plant extracts: A multifaceted approach in photocatalysis, environmental remediation, and biomedicine. *RSC Adv.* **2025**, 15, 3858-3903.
17. Albeladi, S.S.R.; Malik, M.A.; Al-Thabaiti, S.A. Facile biofabrication of silver nanoparticles using Salvia officinalis leaf extract and its catalytic activity towards Congo red dye degradation. *J. Mater. Res. Technol.* **2020**, 9, 10031-10044.
18. Song, J.; Han, G.; Wang, Y.; Jiang, X.; Zhao, D.; Li, M.; Yang, Z.; Ma, Q.; Parales, R.E.; Ruan, Z. Pathway and kinetics of malachite green biodegradation by *Pseudomonas veronii*. *Sci. Rep.* **2020**, 10, 4502-4519.
19. Shankar, A.; Kumar, V.; Kaushik, N.K.; Kumar, A.; Malik, V.; Singh, D. Sporotrichum thermophile culture extract-mediated greener synthesis of silver nanoparticles: Eco-friendly functional group transformation and anti-bacterial study. *Curr. Res. Green Sustain. Chem.* **2020**, 3, 100-119.
20. David, L.; Moldovan, B. Green synthesis of biogenic silver nanoparticles for efficient catalytic removal of harmful organic dyes. *Nanomaterials* **2020**, 10, 202-218.
21. Zahoor, M.; Nazir, N.; Iftikhar, M.; Naz, S.; Zekker, I.; Burlakovs, J.; Uddin, F., Kamran, A.W.; Kallistova, A.; Pimenov, N.; Ali, K.F. A review on silver nanoparticles: Classification, various methods of synthesis, and their potential roles in biomedical applications and water treatment. *Water* **2021**, 13, 2216-2231.
22. Ullah, I.; Khalil, A.T.; Ali, M.; Iqbal, J.; Ali, W.; Alarifi, S.; Shinwari, Z.K. Green-synthesized silver nanoparticles induced apoptotic cell death in MCF-7 breast cancer cells by generating reactive oxygen species and activating caspase 3 and 9 enzyme activities. *Oxid. Med. Cell. Longev.* **2020**, 2020, 1-14.
23. Varadavenkatesan, T.; Vinayagam, R.; Selvaraj, R. Green synthesis and structural characterization of silver nanoparticles synthesized using the pod extract of Clitoria ternatea and its application towards dye degradation. *Mater. Today Proc*. **2019**, 23, 27-29.
24. Punnoose, M.S.; Mathew, B. Treatment of water effluents using silver nanoparticles. *Mater. Sci. Eng.* **2018**, 2, 59-66.
25. Varadavenkatesan, T.; Selvaraj R.; Vinayagam, R. Dye degradation and antibacterial activity of green synthesized silver nanoparticles using *Ipomoea digitata* Linn. flower extract. *Int. J. Environ. Sci. Technol.* **2019**, 16, 2395-2404.
26. Azeez, L.; Lateef, A.; Adebisi, S.A.; Oyedeji, A.O. Novel biosynthesized silver nanoparticles from cobweb as adsorbent for Rhodamine B: equilibrium isotherm, kinetic and thermodynamic studies. *Appl. Water Sci.* **2018**, 8, 1-12.
27. Dihom, H.R.; Al-Shaibani, M.M.; Mohamed, R.M.S.R.; Al-Gheethi, A.A.; Sharma, A.; Khamidun, M.H.B. Photocatalytic degradation of disperse azo dyes in textile wastewater using green zinc oxide nanoparticles synthesized in plant extract. *Water* **2022**, 15, 471-485.
28. Leonida, M.D.; Banjade, S.; Vo, T.; Anderle, G.; Haas, G.J.; Philips, N. Nanocomposite materials with antimicrobial activity based on chitosan. *Int. J. Nano Biomater.* **2011**, 3, 316-334.
29. Devika, R.B.; Varsha, B.P. Studies on effect of pH on cross-linking of chitosan with sodium tripolyphosphate: A technical note. *PharmSciTech,* **2006**, 7, 1-6.

30. Borchert, H.; Shevchenko, E.V.; Robert, A.; Mekis, I.; Kornowski, A.; Grubel, G.; Weller, H. Silver nanoparticles: Large scale solvothermal synthesis and optical properties. *Langmuir* **2005**, 21, 1931-1936.

31. Kwiczak-Yiğitbasi, J.; Laçin, O.; Demir, M.; Ahan, R.E.; Seker, O.S.; Baytekin, B. A sustainable preparation of catalytically active and antibacterial cellulose metal nanocomposites: via ball milling of cellulose. *Green Chem.* **2020**, 22, 455-464.

32. David, L.; Moldovan, B. Green synthesis of biogenic silver nanoparticles for efficient catalytic removal of harmful organic dyes. *Nanomaterials* **2020**, 10, 202-218.

33. Abdulwahid, W.; Abdul, K.; Nursiahla, N.N.; Wayan, S. Synthesis of silver nanoparticles using *Muntingia calabura* L. extract as bioreductor and applied as glucose nanosensor. *Orient. J. Chem.* **2018**, 34, 3088-3094.

34. Nazari, N.; Kashi, F.J. A novel microbial synthesis of silver nanoparticles: its bioactivity, Ag/Ca-Alg beads as an effective catalyst for decolorization Disperse Blue 183 from textile industry effluent. *Separ. Purif. Technol.* **2021**, 259, 118-127.

35. Ashok, K.T.; Vikas, R. Cross-linked Chitosan films: Effect of cross-linking density on swelling parameters. *Pak. J. Pharm. Sci.* **2010**, 23, 443-448

36. Gautam, A.; Rawat, S.; Verma, L.; Singh, J.; Sikarwar, S.; Yadav, B.C.; Kalamdhad, A.S. Green synthesis of iron nanoparticle from extract of waste tea: An application for phenol red removal from aqueous solution. *Environ. Nanotechnol. Monit. Manag.* **2018**, 10, 377-387.

37. Darwish, A.A.A.; Rashad, M.; Al-aoh, H.A. Methyl orange adsorption comparison on nanoparticles: Isotherm, kinetics, and thermodynamic studies. *Dyes Pigments* **2018**, 160, 563-571.

38. Bamgbose, J.T.; Bamigbade, A.A.; Nkiko, M.O. Adsorption kinetics and thermodynamics of malachite green onto chitosan/sodium citrate beads. *Ife J. Sci.* **2013**, 15, 385-398.

39. Lellis, B.; Favaro-Polonio, C.Z.; Pamphile, J.A.; Polonio, J.C. Effects of textile dyes on health and the environment and bioremediation potential of living organisms. *Biotechnol. Res. Innov.* **2019**, 3, 275-290.

40. Bamgbose, J.T.; Bamigbade, A.A.; Nkiko, M.O.; Ahmed, S.A.; Ikotun, A.A. Kinetics and thermodynamic studies of adsorption of malachite green onto unmodified and EDTA-modified groundnut husk. *African J. Pure Appl. Chem.* **2012**, 6, 141-152.

41. Ofudje, E.A.; Sodiya, E.F.; Ibadin, F.H.; Ogundiran, A.A.; Alayande, S.O.; Osideko, O.A. Mechanism of Cu^{2+} and reactive yellow 145 dye adsorption onto eggshell waste as low-cost adsorbent *Chem. Ecol.* **2021**, 37, 268-289.

42. Namasivayam, C.; Muniasamy, N.; Gayathri, K.; Rani, M.; Reganathan, K. Removal of dyes from aqueous solution by cellulosic waste orange peel. *Biores. Technol.* **1997**, 57, 37-42.

43. Nasiri, J.; Motamedi, E.; Naghavi, M.R.; Ghafoori, M. Removal of crystal violet from water using β-cyclodextrin functionalized biogenic zero-valent iron nanoadsorbents synthesized via aqueous root extracts of *Ferula persica*. *J. Hazard Mater*. **2019**, 367, 325-338.

44. Dubinin, M.M. The potential theory of adsorption of gases and vapors for adsorbents with energetically non-uniform surface. *Chem. Rev.* **1960,** 60, 235-266.

45. Rajabi, M.; Mirza, B.; Mahanpoor, K.; Mirjalili, M.; Moradi, O.; Najafi, F.; Sadegh, H.; Shahryari-Ghoshekandi, R.; Asif, M.; Tygi, I.; Agarwal, S. Adsorption of malachite green from aqueous solution by carboxylate group functionalized multi-walled carbon nanotubes: Determination of equilibrium and kinetics parameters. *J. Ind. Eng. Chem.* **2016**, 34, 130-138.

46. Ghaedi, M.; Azad, F.N.; Hajati, S.; Dashtain, K.; Goudarzi, A.; Soylak, M. Central composite design and genetic algorithm applied for the optimization of ultrasonic-assisted removal of malachite green by ZnO nanorod-loaded activated carbon. *Spectrochim. Acta Part A* **2018**, 167, 157-164.

47. Nekouei, F.; Kargarzadeh, H.; Nekouei, S.; Tyagi, I.; Garwal, S.; Gupta, V.K. Preparation of nickel hydroxide nanoplates modified activated carbon for malachite green removal from

solution: kinetics, thermodynamics, isotherm and antibacterial studies. *Process. Saf. Environ.* **2019**, 102, 85-97.

48. Tang, Y.; Zeng, Y.; Hu, T.; Zhou, Q.; Peng, Y. Preparation of lignin sulfonate-based mesoporous materials for adsorbing malachite green from aqueous solution. *J. Environ. Chem. Eng*. 2016, 4, 2900-2910.

49. Yunusa, U.; Ibrahim, M.B. Reclamation of malachite green-bearing wastewater using desert date seed shell: Adsorption isotherms, desorption and reusability studies. *ChemSearch J.* **2019,** 10, 112 -122.

50. Pandian, A.M.K.; Karthikeyan, C.; Rajasimman, M. Isotherm and kinetic studies on adsorption of malachite green using chemically synthesized silver nanoparticles. *Nanotechnol. Environ. Eng.* **2017**, 2, 1-17.

51. Azaman, S.A.H.; Afandi, A.; Hameed, B.H.; Mohd Din, A.T. Removal of malachite green from aqueous phase using coconut shell activated carbon: Adsorption, desorption, and reusability studies. *J. Appl. Sci. Eng.* **2018**, 21, 317-330.